

Thermal decomposition mechanisms of tungsten nitride CVD precursors on Cu(1 1 1)

Yaw-Wen Yang^{a,b,*}, Jin-Bao Wu^{b,c}, Jelin Wang^{b,1}, Yi-Feng Lin^b, Hsin-Tien Chiu^b

^a National Synchrotron Radiation Research Center, 101 Hsin-Ann Road, Hsinchu 30077, Taiwan

^b Department of Applied Chemistry, National Chiao-Tung University, Hsinchu 300, Taiwan

^c Materials Research Laboratories, Industrial Technology Research Institute, Chutung 310, Taiwan

Received 7 December 2004; accepted for publication 2 December 2005

Available online 27 December 2005

Abstract

Chemisorption and thermal decomposition of metallorganic chemical vapor deposition precursors, $(t\text{-BuN})_2\text{W}(\text{NHBu-}t)_2$, bis(*tert*-butylimido)bis(*tert*-butylamido)tungsten (BTBTT) and $(t\text{-BuN})_2\text{W}(\text{NEt}_2)_2$, bis(*tert*-butylimido)bis(diethylamido)tungsten (BTBDT), on Cu(1 1 1) have been investigated by means of thermal desorption spectroscopy (TDS) and synchrotron-based X-ray photoelectron spectroscopy (SR-XPS) under ultrahigh vacuum conditions. The precursors remain intact upon chemisorption on Cu(1 1 1) at 100 K, and at 300 K both precursors decompose readily via the characteristic hydride abstraction/elimination pathways to produce two stable surface intermediates for each precursor. For BTBTT, one species is $\text{W}(=\text{NBu-}t)_3$ and the other is proposed to be a bridged amido complex, $[(t\text{-BuN})_2\text{W}(\mu\text{-NBu-}t)]_2$. In comparison, a W-imine complex and a W–N–C metallacycle are two intermediates produced from BTBDT. Annealing toward 800 K further decomposes the intermediates and the detectable desorption species are completely derived from the ligands. The desorption products from BTBTT include *t*-butylamine generated from α -H abstraction, isobutylene from γ -H elimination, acetonitrile from β -methyl elimination, and molecular hydrogen. In addition to these desorption species, BTBDT produces hydrogen cyanide and imine ($\text{EtN} = \text{CHMe}$) via β -H elimination, not possible with BTBTT due to the absence of β -H in the ligands. Eventually, tungsten nitrides incorporating oxygen atoms and a small amount of graphitic carbons are formed and the stoichiometry is approximated as $\text{WN}_{1.5}\text{O}_{0.1}$. Oxygen incorporation, driven by a large oxide formation enthalpy, is sensitively dependent on the moisture exposure in UHV environment. © 2005 Elsevier B.V. All rights reserved.

Keywords: Synchrotron radiation photoelectron spectroscopy; Thermal desorption spectroscopy; Chemical vapor deposition; Surface chemical reaction; Copper; Tungsten nitrides

1. Introduction

Thin film growth by means of metallorganic chemical vapor deposition (MOCVD) has becoming increasingly popular due to its attractive features of low deposition temperature, high growth rate, and conformal coverage for

nonplanar substrates [1–3]. The latter feature is particularly important to the manufacturing of integrated circuits in which MOCVD is the only deposition technique capable of producing excellent step coverage and high conformality. However, underlying reaction chemistry leading to the thin film growth is rather complex and is far from being completely understood. CVD process takes place in a reaction vessel operating at a pressure of up to several hundred milli-Torr and under this condition both surface reaction and gas-phase reaction can contribute to the film growth significantly. Fortunately, the unique attributes of CVD and the surface chemistry that underlies these features can be investigated by employing a plethora of surface spectroscopic tools [4–7].

* Corresponding author. Address: National Synchrotron Radiation Research Center, 101 Hsin-Ann Road, Hsinchu 30077, Taiwan. Tel.: +886 3 578 0281 7314; fax: +886 3 578 3813.

E-mail address: yang@nsrrc.org.tw (Y.-W. Yang).

¹ Present address: Taiwan Semiconductor Manufacturing Company, Hsinchu 30077, Taiwan.

Metal nitrides are of particular interest in microelectronic device fabrication because of the unusual properties associated with the nitride materials such as high mechanical hardness, high thermal and chemical stability. Titanium nitride is one notable material because of its extensive usage as a barrier film in aluminum metallization. Continuous shrinking of the feature dimension in ultra-large-scale-integrated (ULSI) circuits has mandated a transition from aluminum to copper metallization scheme to keep pace with the device performance enhancement. Titanium nitride is not likely to meet the challenges of effectively isolating Cu from Si. Tungsten nitride presents a potentially viable solution given the existence of several attractive properties including superior adhesion to Cu, amorphous in structure [8], easier removal in chemical mechanical polishing [9]. There appear several reports describing the CVD growth of tungsten nitrides but the uniformity of the films inside the narrow structures is usually not of highest quality. In this regard, it is interesting to note that a highly uniform growth of tungsten nitride can be achieved by atomic layer deposition (ALD) using vapors of ammonia and bis(*tert*-butylimido)bis(dimethylamido)tungsten, (*t*-BuN)₂W(NMe₂)₂ [10]. This precursor has a chemical structure very similar to the ones employed here.

In the present study, we shall report on the thermolysis mechanism of the WN single source precursors, (*t*-BuN)₂W(NHBU-*t*)₂, bis(*tert*-butylimido)bis(*tert*-butylamido)tungsten (BTBTT) and (*t*-BuN)₂W(NEt₂)₂, bis(*tert*-butylimido)bis(diethylamido)tungsten (BTBDT), on a clean Cu(111) surface via synchrotron-based high resolution XPS and thermal desorption spectroscopy performed in UHV environment. These two precursors are isomers, but the latter has two β-Hs while the former has none. This small structural difference facilitates an unambiguous identification of dissociation pathways. An earlier film growth study using the former precursor already suggested that the W=N bond survives better than the W–N bond during thermolysis, thereby preserving the WN portion of the precursor into the cubic WN lattice [11]. Energetics and mechanism involved in the activation and thermal decomposition of the former precursor in *steady growth* regime have been reported based on the work carried out with temperature-programmed reaction spectroscopy and reactive scattering techniques [12]. Thermal decomposition of the same two precursors on Si(100)-(2 × 1) leads to an unexpected formation of tungsten metal [13]. Main emphasis of the present work is thus placed on elucidating the surface reactions occurring in the *early stage* of the tungsten nitride film growth. The obtained results further illuminate the issue of how the molecular structure of precursor governs its decomposition pathways.

2. Experimental

The experiments were performed in a mu-metal ultra-high vacuum chamber with its details described previously [14]. Relevant to the present data acquisition, a quadrupole

mass spectrometer (UTI 100 C) was used for the TDS measurement and a triple-channeltron electron energy analyzer (VG CLAM 2) for the SR-XPS measurement. Photoemission measurements were carried out at the wide range spherical grating monochromator beamline (WR-SGM) at National Synchrotron Radiation Research Center. XPS data were acquired at fixed photon energy of 600 eV to cover all the studied core levels at once instead of optimizing individual core level signal to avoid time-consuming practice of changing grating. Nevertheless, the data quality is still very good and the total instrumental resolution, including the beamline and energy analyzer, was estimated to be better than 0.3 eV. Binding energy (b.e.) scale in all the spectra was referenced to a well-resolved spin-orbit component of bulk Cu 2p_{3/2} peak at 75.10 eV. For brevity, only the energy value of W 4f_{7/2} peak is reported here since the spectrum for the second spin-orbit component, W 4f_{5/2}, is a mere duplicate.

Thermal desorption experiments were performed with a quadrupole mass spectrometer differentially-pumped by a separate 70 l/s turbo pump. The ionizer in the mass spectrometer was enclosed by a copper, liquid nitrogen shroud to reduce both hydrocarbon background and thermal heating in the ionizer. A linear heating rate of 3 K/s was normally used. Mass spectrometer was multiplexed via software control to monitor up to fifteen ions recorded simultaneously based on a digital counting scheme. Principal component analysis [15] was used to extract the number of independent ions (nonrelated through mass fragmentation process) existing in a given set of TDS spectra. This technique originated from linear algebra is very useful in narrowing down the number of possible desorption products and its application in TDS has been described in our previous work [14].

The Cu(111) sample was fastened with tungsten wires to the copper feedthroughs welded to the end of a stainless steel liquid nitrogen Dewar. The Cu(111) crystal was cleaned by a standard procedure of repeated argon ion sputtering and UHV annealing. The surface cleanliness was verified by XPS and the crystallographic order was verified by LEED. Both BTBTT and BTBDT precursors were synthesized based on the modification of a previously published procedure [16]. Before use, the precursors were stored in a dry, oxygen-free environment. The *t*-butylamine and diethylamine, purchased from Aldrich, were used without any further chemical purification and, before being admitted into the vacuum chamber, were subject to several freeze-pump-thaw cycles. Dosing was done with a 3.2 mm diameter glass doser terminated with a 0.5 mm pinhole. Gas manifold was constructed from glass as much as possible to minimize the precursor decomposition on metallic parts during the precursor transfer to the sample. Immediately prior to the dosing, the headspace in the precursor reservoir was evacuated again to remove any volatile amines accumulated from precursor decomposition. Surface exposures are reported in langmuirs (1 L = 1 × 10⁻⁶ Torr s) but without correcting for ion gauge sensitivity difference.

3. Results

MOCVD method provides a versatile approach for preparing thin films; however, an incomplete removal of the ligands in the precursor during the growth can be the source of contamination in the films, thereby compromising the film properties. Due to the thermal lability of the present precursors, amines can be produced and then carried over to the growth surface. The coadsorption of the amines and precursor can complicate the spectroscopic analysis. In order to differentiate the precursor contribution from amine contribution, individual adsorption studies of *t*-butylamine and diethylamine on Cu surface were undertaken first. The more comprehensive results of amines adsorption on Cu surface will be published elsewhere and thus only results pertinent to the precursors are reported here.

3.1. Diethylamine and *t*-butylamine

Fig. 1 shows the multi-mass TDS spectra for the diethylamine adsorbed on Cu(111). Mass to charge ratios of 58 (a predominant fragment of the parent ion at 73 Th), 56, 41, and 2 are presented in (a)–(d). The thomson (Th) is the m/z unit and used throughout the paper. The desorption peak at 150 K, common among all the fragments, is due to the physisorption species. The molecular desorption resulting in 58 Th fragment is almost complete before reaching room temperature, signifying the weak chemisorption of diethylamine on Cu(111). The 56 Th species is a fragment of the parent ion but its desorption trace

deviates significantly from that of 58 Th species for temperature higher than 280 K, indicating the existence of a second source producing 56 Th fragment. Imine, $C_2H_5NC_2H_4$ (*N*-ethyl-ethanimine, 71 Th), can be formed as the adsorbed diethylamine undergoes a β -H elimination on Cu(111). Therefore, the 56 Th feature at temperature higher than 280 K is attributed to the imine. The 41 Th signal is mostly derived from 56 Th but the possibility of forming a small amount of acetonitrile (41 Th) at higher temperature of 350 K cannot be ruled out. Desorption of H_2 occurs from 320 to 440 K, higher than 280–350 K normally found for hydrogen chemisorbed on Cu(111) [17,18]. Higher desorption temperature suggests that the hydrogen originates from C–H bond cleavage taking place at higher temperature. For comparison, the molecular desorption for *t*-butylamine preadsorbed on Cu(111) is also shown in Fig. 1e. In addition to the desorption of the physisorption state at 140 K, other molecular desorption states at 205 and 260 K exist. Overall desorption profiles of two amines are rather similar (Fig. 1a and e), all exhibiting weak chemisorption except that *t*-butylamine binds to the Cu surface slightly stronger. The observation of amine adsorption in predominantly molecular form agrees with the result from an earlier study [19].

Amines can also dissociatively chemisorb on Cu(111), though not to a large degree. Fig. 2 shows the change of N 1s (A) and C 1s (B) XPS spectra for a 4 ML of diethylamine adsorbed on Cu(111) surface at 100 K and then annealed to higher temperatures. Here, one ML is simply defined as the amount of amine needed to cover the substrate surface with the chemisorbed amine. For physisorbed diethylamine (100 K spectrum), N 1s and C 1s core levels appear as broad peaks at 400.3 and 286.7 eV, respectively. As the surface is heated to 200 K, only chemisorbed diethylamine remains on Cu surface, producing N 1s at 399.8 eV and C 1s at 285.9 eV. Previous XPS studies of the adsorption of alkylamines on Ni, Fe and W thin films indicate that organic amines adsorb on metal surfaces through their nitrogen lone pairs and exhibit a characteristic N 1s b.e. from 400.1 to 399.7 eV, depending on the number of alkyl groups in the amines [19]. Our b.e. values for diethylamine and the *t*-butylamine agree well with the reported data. An annealing to 300 K desorbs most of the diethylamine and leaves behind 13% N and 20% C relative to those on 200 K on the surface, consistent with the weak chemisorption nature of the amine. The 300 K annealing also produces a new species with N 1s at 398.2 eV and C 1s at 284.7 eV. After annealing to much higher temperatures, two carbon peaks merge into a major one at 284.5 eV, attributed to graphitic carbon [20].

In comparison, the two-peak feature in the N 1s spectra is retained up to 800 K, with a larger one at 398.4 eV and a smaller one at 400.3 eV. A direct bonding of nitrogen and carbon species to copper surface forms nitride and carbide species with their b.e. lower than 397 and 283 eV, respectively [20]. Our observed N 1s and C 1s b.e. values are higher than those values, indicating that the formation of

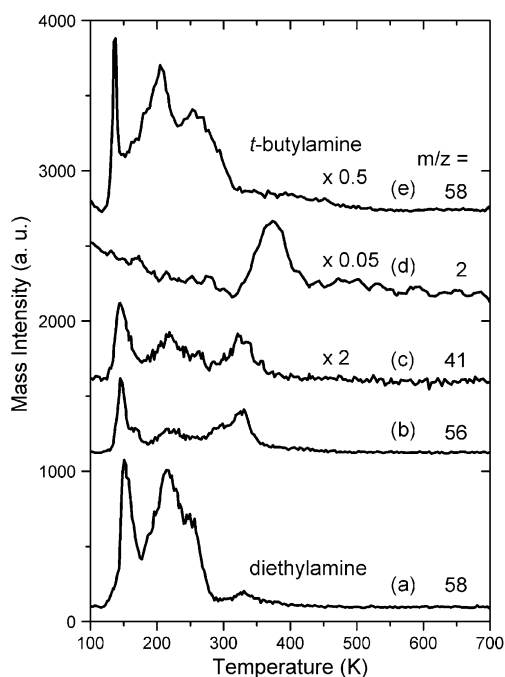


Fig. 1. Multimass TDS spectra after adsorbing 7 L of diethylamine (a–d) on Cu(111) at 100 K. Also shown is the TDS for 7 L of *t*-butylamine adsorbed under the same condition (e).

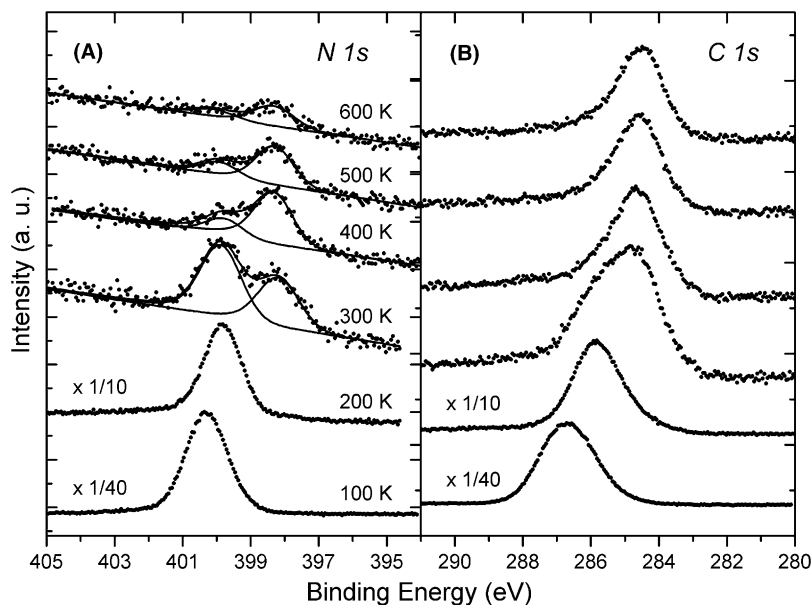


Fig. 2. Change of N 1s (A) and C 1s (B) core level spectra with the annealing temperature for ~ 4 ML of diethylamine adsorbed on Cu(111). The spectra were acquired with X-ray of 600 eV in energy.

copper nitride and copper carbide is not the case. Instead, the formation of carbonitride on the surface seems more likely. Many studies of carbon nitride film, with an aim of growing super hard β - C_3N_4 phase, have been available and two major N 1s peaks at 398.1–398.4 eV and 400.3–400.7 eV are often reported [21–23]. The former peak is interpreted as originated from nitrogen bonded to sp^3 carbons and the latter peak corresponds to nitrogen in a sp^2 carbon environment. However, in view of lower temperature and lower coverage employed here, three dimensional sp^3 bonding between carbon and nitrogen may not be easily realized on the surface. It seems more reasonable to assign the observed 398.4 eV peak to nitrile ($C\equiv N$) species [24] instead of nitrogen bonded to sp^3 carbons in carbonitride, and the observed 400.3 eV peak to nitrogen in a sp^2 carbon such as graphite. As for the *t*-butylamine adsorption on Cu(111), the change of N 1s and C 1s core level spectra with annealing temperature is rather similar to that for diethylamine, hence omitted entirely.

3.2. BTBTT precursor

Before presenting TDS data for the precursor, few words will be said about the mass identification. The molecular desorption of BTBTT (470 Th) cannot be directly probed because the mass range for the present mass spectrometer is limited to 300 Th. The mass ionization pattern of BTBTT resulted in a rich series of mass fragments that was documented by the GCMS. Among the fragments, the one with a mass-to-charge ratio (m/z) of 230 was found to be a major W-containing species and chosen to represent the BTBTT molecule, a practice adopted in the previous reactive scattering study of BTBTT also [12]. The observation of the desorption of W-containing species

is possible only after a completion of the chemisorbed BTBTT layer, and the desorption species from the chemisorbed BTBTT are exclusively derived from the ligands, as evidenced by a constant W 4f signal throughout different annealing temperatures (see XPS data below). The recombinative desorption of the ligands was also investigated and concluded to be nonexistent, judged by the absence of higher mass signals at up to twice the mass to charge ratio of the ligands. Consequently, the desorption spectra of the precursors can be fully accounted for by considering their constituent ligands only in spite of the seeming complexity of the precursor.

Fig. 3 shows the multimass TDS spectra obtained for a ~ 5 ML of BTBTT adsorbed on Cu(111) at 100 K. One ML is simply defined as the amount of BTBTT needed to complete the chemisorption layer. For clarity, truncated spectra are presented with a temperature break at around 270 K where an intense desorption peak due to physisorption state is found. The species with $m/z = 58$ is the heaviest fragment observable for *t*-butylamine because the parent ion at 73 Th is absent in the fragmentation pattern [25]. The intense feature preceding the physisorption desorption peak at 270 K is entirely due to coadsorbed *t*-butylamine. Coadsorption of the amines and precursor can only be minimized but not completely eliminated because of the relative ease of precursor decomposition upon contact with the metallic passage inside the gas manifold. Beyond 270 K, *t*-butylamine evolves continuously all the way up to 600 K, which must be originated from BTBTT precursor because the desorption of amine alone is completed before reaching 350 K. The desorption of $m/z = 56$ species occurs in two broad peaks at 515 and 575 K. The fraction of this species derived from the fragmentation of *t*-butylamine can be neglected, as evidenced by the absence

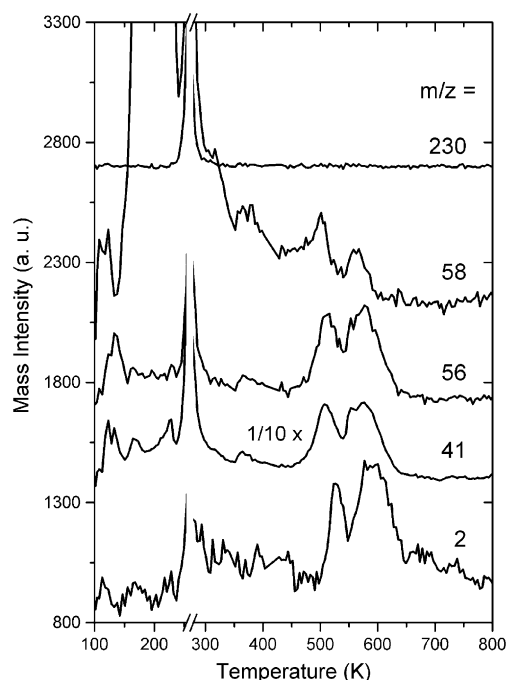


Fig. 3. Multimass TDS spectra for an about 5 ML of BTBTT adsorbed on Cu(111). The intense feature before 270 K peak for 58 Th desorption curve is due to coadsorbed *t*-butylamine ligand. The species with $m/z = 230$ represents a major fragment of BTBTT precursor and the other masses are all derived from the ligand side of the precursor.

of desorption peak before 270 K where an intense *t*-butylamine desorption occurs. Therefore, the observed $m/z = 56$ species is attributed to isobutylene entirely.

The next lighter species is acetonitrile (CH_3CN , parent ion at 41 Th). The mass intensity ratio between 41 Th fragment and its massive parent ion is listed as 2.5 for isobutylene (56 Th) and as 0.2 for *t*-butylamine (58 Th) [25]. The observed $m/z = 41$ signal is very large (at least five times larger than 56 Th signal), which immediately warrants a valid assignment of acetonitrile. Next lighter species is to be composed of either two carbon atoms or one carbon and one nitrogen atom (HCN). Even enlisting the help from PCA analysis, we found very little evidence to support the finding of HCN and ethylene, consistent with the earlier finding [12]. Methane, a likely product owing to the prevalence of methyl elimination that is required to explain the production of acetonitrile, can only be detected at high precursor coverage. Finally, a major desorption of H_2 is found between 480 and 650 K. Interestingly, the desorption profile of H_2 bears a resemblance to those of *t*-butylamine and isobutylene, pointing to the correlated nature of the reaction and desorption processes.

It is known that core level XPS data contain a wealth of information; therefore, a nonlinear least squares curve-fitting is relied upon to extract as much information as possible. We usually used a linear background in conjunction with a line shape function generated by a convolution of Gaussian function with the Doniach-Sunjic function broadened by a finite lifetime. In a given spectrum, the

Gaussian with (Γ_G), Lorentzian width (Γ_L) and Doniach-Sunjic asymmetric parameter (α) were allowed to vary in the fits but were constrained to be the same for all the peaks. However, for the spectra acquired after high temperature annealing, a slight variation of peak characteristics is allowed to account for the physical property change of the species. Reliable peak fitting of N 1s spectra could be carried out because of a limited number of nitrogen species existing in the precursor molecule. In comparison, a meaningful fitting of C 1s spectrum could not be done usually because of the uncertain number and uncertain chemical structures of species. Fortunately, a great deal of information can be learned from carefully analyzing W 4f and N 1s spectra.

Fig. 4 shows the change of W 4f (A), N 1s (B), and C 1s (C) XPS spectra with the annealing temperature for one ML of BTBTT adsorbed on Cu(111). An initial dose at 100 K produces a well-defined W 4f spin-orbit doublet with the W 4f_{7/2} at a b.e. of 34.1 eV, attributed to chemisorbed BTBTT. Raising the surface temperature to 200 K does not change the spectra. The assertion of a molecularly intact chemisorbed BTBTT is supported by the following observations: (1) The species has a narrowest width among the observed tungsten peaks and can only appear after a full passivation of the gas manifold, suggesting that the species is not due to a mixture of the BTBTT and its partially decomposed products. (2) The total intensity of W 4f peaks remains constant throughout the annealing, validating the assertion that no physisorbed BTBTT component exists in the spectra. For fitting W 4f spectra, the spin-orbit-splitting is set at 2.15 eV and an intensity ratio for the two components of the doublet is fixed at its statistical value of 4:3. For reference, previous studies have derived at the following parameters based on the studies of core level shift on W(110) surface: $\Gamma_L = 0.07$ eV, $\Gamma_G = 0.07$ eV, $\alpha = 0.06$ [26,27]. Shown underneath each raw spectrum in Fig. 4 are the fitted components and resultant curves. The quality of the fit is excellent and the derived parameters for W 4f are typically as follows: $\Gamma_L = 0.1$ eV, $\Gamma_G = 1.0$ eV, and $\alpha = 0.05$. The derived Gaussian width is much larger than the instrumental width of 0.3 eV, suggesting the presence of other broadening factors such as the vibrational excitation accompanied by the electronic transition in the precursor molecules.

A warmup to 300 K produces a dramatic change in all three core-level spectra, notably the shift of spectrum centroid toward lower b.e. This change defies understanding because a copper surface at room-temperature is generally regarded as nonreactive. Moreover, the 300 K W 4f spectrum, particularly in the valley region between two spin-orbit doublets, is found to be sensitively dependent on the moisture exposure during spectrum acquisition even in UHV. The moisture accelerates the formation of multiple tungsten oxides of unspecified chemical states, driven by the large formation enthalpies of the oxides. Thus, another controlled experiment carried out at 300 K was performed in an aim to eliminate the oxide interference.

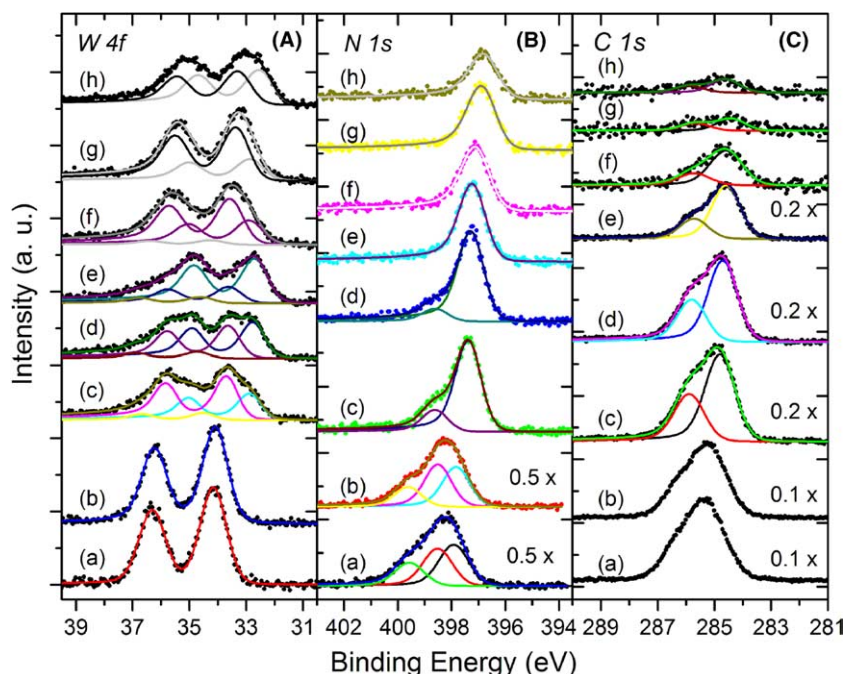


Fig. 4. Change of W 4f (A), N 1s (B) and C 1s (C) XPS spectra with annealing temperature for a one ML of BTBTT initially adsorbed on Cu(111) at 100 K. The raw data, after subtracting the fitted linear background, are depicted in solid circles; the component and resultant curves derived from the peak fitting are also plotted together. The photon energy was set at 600 eV. The annealing temperature for each curve is (a) 100 K, (b) 200 K, (c) 300 K, (d) 400 K, (e) 500 K, (f) 600 K, (g) 700 K, and (h) 800 K.

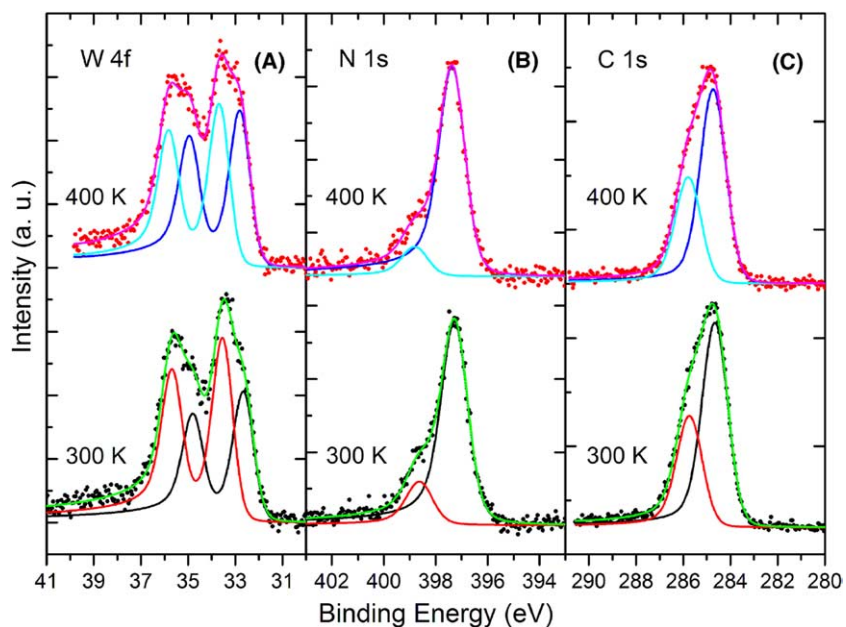


Fig. 5. W 4f (A), N 1s (B) and C 1s (C) XPS spectra for Cu(111) saturated with BTBTT precursor at 300 K and later annealed to 400 K. The dosing at room temperature was meant to eliminate tungsten oxides formed between the precursor and moisture. A fitted linear background was subtracted from the raw data and the same photon energy of 600 eV was used.

Fig. 5 shows W 4f (A), N 1s (B), and C 1s (C) XPS spectra acquired at higher energy-resolution settings on the Cu(111) saturated with BTBTT at 300 K first and later annealed to 400 K. O 1s spectra (data not shown) shows the absence of oxygen at 300 K but the presence of a small

amount of oxygen at a b.e. of 530.5 eV at 400 K. This confirms again that the amount of oxide is intimately related to water moisture, only exacerbated in cryogenic measurements. Careful fitting reveals a clear existence of two W 4f_{7/2} peaks at 32.8 and 33.6 eV, with none of them

resembling chemisorbed BTBTT. Two N 1s peaks are resolved and located at 397.3 and 398.6 eV, with an intensity ratio of 4.7:1. Two fitted C 1s peaks are at 284.8 and 285.8 eV and they are assigned to three methyl carbons and one central carbon of the *t*-butylamine ligand, respectively. Annealing to 400 K increases W 4f intensity in the low b.e. side and produces little change in both N 1s and C 1s spectra, consistent with TDS data that indicate the ligand decomposition does not begin until a higher temperature of ~450 K is reached. It is emphasized that at 300 K the chemisorbed precursor already transforms into different forms and a conjecture about their structures is to be presented in the discussion section.

Having recognized the subtle transformation undergone by the precursor at 300 K, we now return to Fig. 4 and continue to present thermal annealing effect on the spectra. As a mandatory practice to prevent oxide formation, the ambient temperature of the sample was raised to 300 K by blowing away liquid nitrogen coolant right after two cryogenic data runs. The 100 K N 1s spectrum has a third component at 399.5 eV attributed to co-adsorbed *t*-butylamine that also contributes to C 1s signal. For the W 4f spectrum at 300 K, besides two aforementioned peaks at 32.8 and 33.6 eV, one additional peak at 34.5 eV, attributed to tungsten oxide, is also resolved. In comparison, the b.e. of W 4f_{7/2} is listed as 32.8 eV for WO₂ and 35.8 eV for WO₃ [20].

After annealing to 500 K, slightly beyond the desorption onset, no major changes are to be expected. The lower b.e. side of the W 4f spectrum increases in intensity; N 1s spectrum retains its main peak at 397.2 eV but gradually loses its minor peak at 398.6 eV; C 1s peak continuously drops in intensity without much change in the peak shape. By comparison with TDS spectra, an annealing temperature of 600 K should complete the desorption process to a significant degree; thus a drastic change in all the XPS spectra

is expected. Most notable is the observation of a precipitous drop of C 1s intensity, yet the N 1s intensity decreases only slightly. This observation agrees with the finding of a major desorption of isobutylene. After 800 K, all the volatile thermal decomposition products would have been desorbed, leaving behind stabilized tungsten nitride products with stoichiometry perhaps similar to the common nitrides of W₂N and WN. The final products have their W 4f_{7/2} b.e. at 32.5 and 33.2 eV, but N 1s is at the same b.e. of 396.7 eV. For C 1s spectrum, a major peak is located at the energy position of graphite, i.e. 284.6 eV and a minor peak at 285.8 eV. An oxide peak located at 530.5 eV (spectrum not shown) is found to grow with time slowly. For the ease of referencing, the b.e. values for the major species discovered for BTBTT as well as those for BTBDT are compiled in Table 1.

3.3. BTBDT precursor

BTBDT molecule contains two *t*-butylimido and two diethylamido ligands bonded to central W atom to produce two W=N and two W–N bonds. The relatively weaker W–N bond is believed to break first. Fig. 6 shows multimass thermal desorption spectra for about 2 ML of BTBDT adsorbed on Cu(111). The species with *m/z* = 286 represents a major W-containing fragment of BTBDT precursor. The desorption peak at 265 K is attributed to the physisorption state and again can only be observed after a thorough passivation of the gas manifold. The desorption feature preceding 265 K is due to the coadsorbed ligands and thus only the features after 265 K will be discussed. The mass to charge ratios of the diethylamine and *t*-butylamine parent ions are the same as 73 but the largest, observable fragment of *t*-butylamine is only 58 Th. The desorption of *m/z* = 73 species starts right after the physisorption desorption peak and gradually tapers off in higher temperatures.

Table 1
Binding energies of various species formed during the heating of precursors

	BTBTT			BDBTT		
	W 4f _{7/2}	N 1s	C 1s	W 4f _{7/2}	N 1s	C 1s
Chemisorbed	34.1	397.9 (imido) 398.5 (amido)	284.8 285.8	34.0	397.6 (imido) 398.3 (amido)	
Intermediates at 300 K	32.8 (1) ^a 33.6 (3) ^a 34.4 (oxide)	397.3 (W=N) 398.6	284.8 (*Me ₃ CN) 285.8 (Me ₃ *CN)	32.8 (4a?) ^a 33.4 (4b?) ^a 34.9 (oxide)	397.2 (W=N) 398.6	284.6 286.7
WN _x O _y after 800 K ^c	32.5 33.2	396.7	284.5 285.8	32.0 32.8 34.2	397.0 397.8	283.8 284.5 285.8
^b	32.0 (W ₂ N) 32.4 (WN) 33.3 (WN ₂)	397.9 (W ₂ N) 397.5 (WN) 397.4 (WN ₂)				

O 1s b.e. of final tungsten nitrides is at 530.5 eV.

^a Arabic numerals refer to the species in the reaction scheme presented in Discussion Section.

^b The data are from Ref. [42].

^c The stoichiometry of the nitrides produced is WN_{1.5}O_{0.1}C_{0.4} for BTBTT, and WN_{1.3}O_{0.2}C_{0.8} for BTBDT. However, the carbon is mostly in graphitic form and not incorporated into nitride products.

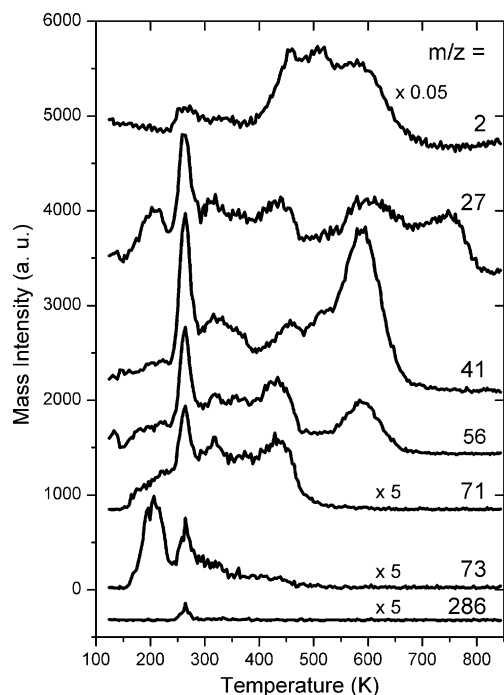


Fig. 6. Multimass TDS spectra for an about 2 ML of BTBDT adsorbed on Cu(111). The species with $m/z = 286$ represents a major fragment of BTBDT and the other masses are all derived from the ligand side of the precursor.

Above 450 K, no diethylamine desorption can be observed. The desorption of $m/z = 58$ species is similar to that of diethylamine and is hence omitted.

The species with $m/z = 71$ has desorption features different from those of $m/z = 73$ species, i.e. a substantial desorption in the high temperature side. Three broad desorption features are found with the most intense one occurring at 430 K. The 71 Th species is assigned to imine, $\text{EtN} = \text{CHMe}$, formed via a β -H elimination (N atom regarded as α site) accompanied by W–N bond cleavage. It is noted that the imine species is derived from the diethylamido, not from *t*-butylimido ligand, owing to the absence of β -H in the latter. By the same token, no imine desorption can be detected for BTBTT precursor because of all *t*-butyl groups used in making the ligands. The next lighter species detected has an $m/z = 56$, with a negligible contribution from the fragmentation of both *t*-butylamine and diethylamine, as evidenced by the absence of desorption peak before 265 K where the intense amine desorption is noted. However, the contribution of imine to 56 Th species cannot be ascertained because of the lack of mass fragmentation data of imine species. Nevertheless, a unique desorption feature, not found in the higher-mass desorption spectra, exists in the high temperature region between 480 and 660 K. This high temperature desorption feature, centered at around 590 K, is entirely due to the isobutylene.

Clear evidence can be found to support the observation of acetonitrile and hydrogen cyanide desorption at higher temperature. The desorption trace of 41 Th contains a disproportionately large signal in the temperature region

higher than 440 K, as compared with the desorption trace of 56 Th. It is thus concluded that acetonitrile desorbs at temperature over 440 K with its peak desorption temperature at 585 K. The desorption of HCN can also be unequivocally established by the appearance of desorption signal at temperature higher than 650 K where no contribution from higher masses is found. Unlike the case of BTBTT precursor where a clean-cut desorption of HCN cannot be concluded, the pronounced HCN desorption found in BTBDT is presumably related to the straight chain nature of diethylamido ligand. Finally, hydrogen desorption encompasses a wide temperature range up to 700 K, overlapping with the desorption features of all the species but HCN.

Fig. 7 shows the change of W 4f (A), N 1s (B), and C 1s (C) XPS spectra with annealing temperature for 1 ML of BTBDT initially adsorbed on Cu(111) at 100 K. Also shown are the component and their sum spectra derived from the curve fitting. The evolution of the all three core levels with annealing temperature is similar to what is observed for BTBTT other than some subtle spectral difference. The 100 K W 4f spectrum is deemed to be composed of one single component despite the less-resolved feature, as compared to the BTBTT spectrum of 100 K shown previously in Fig. 4(A). The spectral broadening caused by physisorbed BTBDT is ruled out due to a constant W 4f intensity for all the spectra. The worsening of spectral resolution was mainly caused by the malfunctioning analyzer when the data were taken. The Gaussian width, dominated by instrumental broadening, was increased from 1.0 to 1.3 eV. The fitted single component—i.e. molecularly-intact chemisorbed BTBDT—has its W 4f_{7/2} core level located at 34.0 eV. A warmup to 200 K makes little change to the spectra. However, a warmup to 300 K changes the W 4f spectra dramatically, similar to the BTBTT case, and produces stronger electron emission signal in both sides of the main peak. Curve fitting reveals three W 4f_{7/2} components with their b.e. located at 32.8, 33.4 and 34.9 eV. The 34.9 eV peak is due to tungsten oxide and, in comparisons, the oxide formed from BTBTT has a lower b.e. of 34.5 eV. It is found that BTBDT tends to be more susceptible to oxidation, as evidenced by a larger oxide signal and a higher degree of oxidation manifested in higher W 4f_{7/2} b.e. Further annealing results in a greater distortion of W 4f signal and the broad doublet found for BTBTT at all the temperatures is replaced by a featureless hump for BTBDT. Only when heating above 800 K is a distinct W 4f doublet restored.

In contrast with the dramatic change found for W 4f signal, the change in both N 1s and C 1s spectra seems to be more straightforward and bears a strong resemblance to what is observed for BTBTT. For instance, N 1s spectrum of 100 K can be resolved into three components at 397.6, 398.3, and 399.9 eV, corresponding to W=N, W–N, and coadsorbed amine, respectively. When warming up from 200 to 300 K, N 1s spectrum undergoes the similar change, namely, a shift toward lower b.e. as well as an intensity

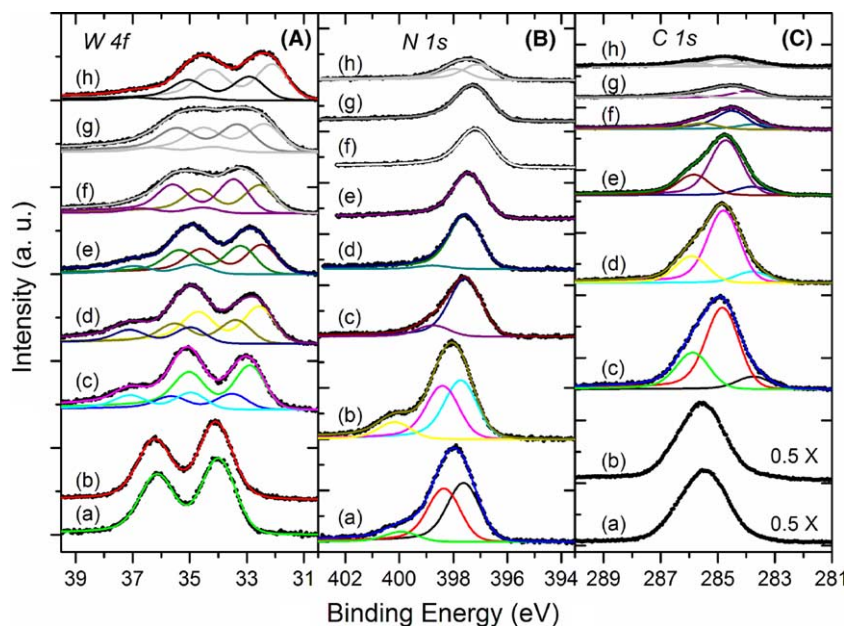


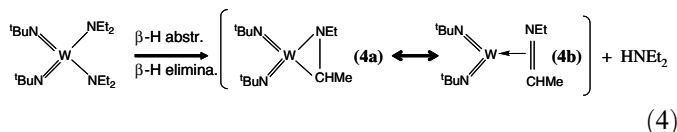
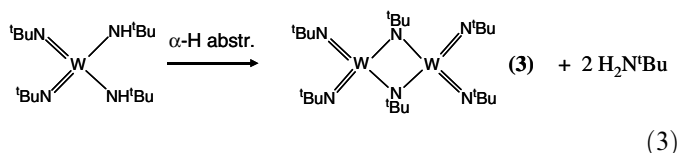
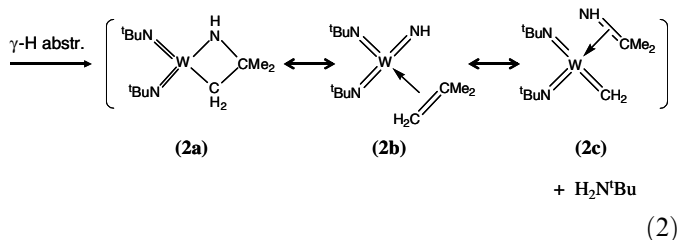
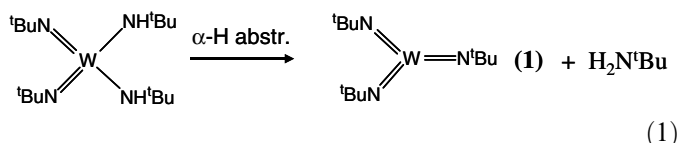
Fig. 7. Change of W 4f (A), N 1s (B) and C 1s (C) XPS spectra with annealing temperature for a one ML of BTBDT initially adsorbed on Cu(111) at 100 K. The annealing temperature for each curve is (a) 100 K, (b) 200 K, (c) 300 K, (d) 400 K, (e) 500 K, (f) 600 K, (g) 700 K, and (h) 850 K.

increase in low b.e. side. Heating toward higher temperature gradually reduces the N 1s intensity and, at the completion of 850 K annealing, N 1s peaks settles at 397.0 and 397.8 eV, deviated from 396.7 eV found for BTBTT. For the C 1s spectra, the intensity decrease spreads out over a wider temperature range, different from BTBTT case where a precipitous drop of carbon intensity is found at 600 K, but consistent with the TDS data of BTBDT where a higher desorption temperature is required (780 vs. 630 K). After 850 K annealing, most carbon species appears at a b.e. of 284.8 eV, same as BTBTT.

4. Discussion

Common tungsten nitrides have chemical formulae as W_2N , WN, etc. The present precursors have higher nitrogen to tungsten and carbon to tungsten ratios than are required to form the aforementioned compounds; as a result, during the thermolysis the precursors continuously discharge the excessive nitrogen and carbon atoms and develop multiple nitrogen to tungsten bonds. Before we discuss the thermolysis process in detail, it is worthwhile to examine the intermediate species formed at 300 K closely because they offer a glimpse of the propensity of bond breaking. As evidenced by b.e. change of W 4f and N 1s core levels and the evolution of amine, a partial decomposition of the precursors already takes place at 300 K. A careful XPS spectrum fitting reveals the existence of two hitherto unknown tungsten compounds and a tungsten oxide, with the discussion on oxide deferred to later section. Based on the common hydride abstraction and hydride elimination pathways [28,29], we propose the following four reaction schemes to explain the formation of

the intermediates and amines based on a plausible assumption that the bond scission occurs between amido ligand and tungsten atom.



Reactions (1)–(3) apply to the BTBTT activated on Cu(111), whereas reaction (4) apply to the BTBDT. Reaction (1) describes a α -H abstraction by one amido ligand, a discharge of *t*-butylamine, and the formation of a third W=N bonds. The reductive elimination of *t*-butylamine

ligand can only be carried out by another neighboring amido ligand, not by surface-adsorbed H atom because of low H adatom concentration owing to the weak chemisorption property of H₂ on Cu(111) [17,18]. Reaction (2) depicts a γ -H abstraction to yield a 4-ring, W–N–C–C metallacycle (**2a**) and a release of *t*-butylamine. Also depicted are two possible resonance structures: (**2b**) and (**2c**) of the metallacycle. It is noted that the relative energies among these three species are not readily known. Reaction (3) represents a coupling of two BTBTT molecules through two bridging amido ligands to form a new complex, [(*t*-BuN)₂W(μ -NBu-*t*)₂], and a resultant release of two *t*-butylamine ligands. For BTBDT, reaction (4) describes an abstraction of β -H from the neighboring diethyl groups followed by the elimination of diethylamine and the formation of a W–N–C metallacycle (**4a**). A similar β -H elimination of BTBDT leads to a W-imine complex (**4b**) from which imine (EtN = CHMe) can be eliminated via dissociation. Again, (**4a**) and (**4b**) can be related through a resonance denoted by a double-headed arrow. During the annealing of BTBDT to 450 K, more imine is formed than diethylamine (cf. $m/z = 71$ with $m/z = 73$ curves of Fig. 6). The coupling reaction for BTBDT, similar to the reaction (2), is deemed unlikely because of the required breaking of N–Et bond to form a bridging amido. The scission of N–C bond has to await a higher temperature, as revealed by TDS data.

Several comments regarding the conjectured metallacycles are in order. There has been the reported synthesis of both W–N–C and W–N–C–C metallacycles [30,31], but none of them have been reported under thin film growth condition perhaps due to the scarcity of their studies. In comparison, there have been many studies of MOCVD growth of TiN due to their extensive use in aluminum interconnect, and the structure analogy between WN and TiN intermediates can be perhaps drawn. For instance, Ti–N–C metallacycle proposed in TiN CVD growth is well accepted [32–35] and subject to several theoretical investigation [36,37]. Moreover, a bridged Ti complex of the structure similar to species (**3**), [Ti(μ -NBu-*t*)(NMe₂)₂]₂, is stable in ambient condition and titanium nitride thin films produced from the decomposition at elevated temperatures contain a significant amount of carbon and oxygen [32]. Besides the 3-ring metallacycle, intermediates of the N-bonded Ti-imine complex [38] and Cr-imine complex [39] have also been proposed separately; whose analogy in tungsten nitride is presented in the reaction (4). A general consensus regarding the metallacycle is that, once formed, it will lead to a carbonitride film due to the difficulty in breaking the cyclic Ti–N–C bond [36,37].

Valuable insight can be gained from an in-depth analysis of high resolution XPS data. Firstly, the four listed reactions show that one amido ligand is liberated for every precursor molecule that has four ligands to begin with. The percentage of the liberated ligands eventually desorbing from the Cu(111) is estimated as 87% (Fig. 2). As a result, N 1s signal is expected to decrease by 22% ($=0.87 \times 0.25$) after the completion of the reactions. The observed de-

crease of N 1s signal, excluding the signal from the coadsorbed *t*-butylamine, is equal to 30% for BTBTT (cf. spectra (a) and (c) in Fig. 4B) and 32% for BTBDT (cf. spectra (a) and (c) in Fig. 7B), close to the expected value, suggesting the plausibility of listed reactions. Secondly, all the proposed decomposition routes result in an increasing fraction of imido ligand, consistent with the formation of a dominant N 1s peak at 397.2 eV. The other minor peak is ascribed to amido-like ligand in the proposed intermediates. This b.e. shift with the bond order forms the basis of our empirical observation of the correlation of bond distance with the XPS N 1s b.e. [40].

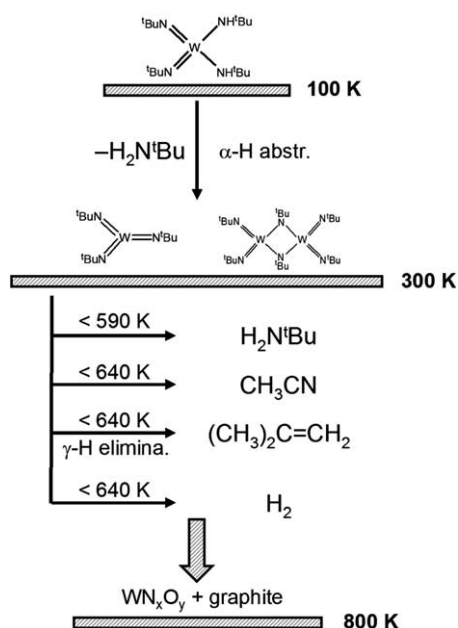
The proposed reaction schemes can be sorted out further, considering only two W peaks are observed for 300 K BTBTT. Species (**2a**) together with their resonance forms of (**2b**) and (**2c**) are the least favored ones owing to their uncertain existence and the observation of negligible amount of carbide (b.e. <284 eV) after 800 K annealing. The N 1s intensity ratio between imido and amido-like is determined to be 4.7:1 from Fig. 5B. Thus, the number ratio between the species (**1**) and (**3**) can be calculated straightforwardly. This number ratio, (**1**)/(**3**), is calculated to be 1.8:1, thereby yielding an intensity ratio of 0.9:1 for two W peaks, as compared to the observed 0.7:1 values. Despite this disappointment at numerical discrepancy, the W 4f b.e. assignment of two species can be made by reasoning how W 4f and N 1s peaks change intensity when BTBTT is heated from 300 to 400 K. The W 4f_{7/2} b.e. of the species (**1**) is at 32.8 eV, whereas the W 4f_{7/2} b.e. of the species (**3**) is at 33.6 eV, consistent with the chemical intuition of associating smaller electronegativity with the doubly-bonded nitrogen atoms. For BTBDT, the plausible decomposition route leads to two species denoted as (**4a**) and (**4b**). Unfortunately, no sure assignment of W 4f_{7/2} b.e. can be made because of the uncertain effect of chemical structure difference on the b.e. of W 4f core level.

As the intermediates are heated toward higher temperatures, a sequence of characteristic bond-breakings occurs, producing distinct reaction products. It is emphasized that not all the reaction products will end up desorbing from Cu(111). For instance, a previous study has shown that free radicals such as CH₃, CH₂, CH remain on Cu(111) and undergo further dehydrogenation at higher temperatures [41]. TDS data in Fig. 3 seem to imply that the reaction products such as isobutylene, acetonitrile, and hydrogen desorb from Cu(111) in a concerted fashion, producing rather similar desorption profiles. This similarity might suggest that the energetics involved in the rate-determining steps of surface bond-breaking processes does not differ much. Isobutylene is produced from γ -H elimination of *t*-butylamido and a W–NH bond is developed afterwards. This reaction channel is very effective in reducing carbon contents, in accord with the observed precipitous drop of C 1s intensity at 600 K. The observation of acetonitrile desorption is explained by two β -methyl elimination steps accompanied by a W–N bond breaking. The detached methyl radicals mostly stay on the surface and undergo

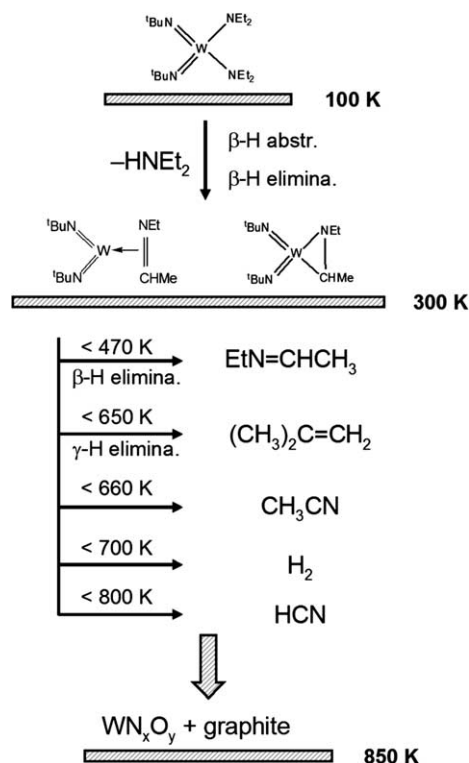
further dehydrogenation, instead of recombining with H atom to desorb as methane. This lack of the methane desorption is in stark contrast with the reactive scattering study of BTBTT from WN_x -coated substrate by Crane et al. [12], where the methane production is found between 450 and 700 K. We believe this difference is due to a lower precursor coverage in use here, which makes available bare Cu sites for a further dehydrogenation of C_1 radicals. The overall thermal decomposition pathways of BTBTT are summarized in Scheme 1.

For the BTBDT, more products are found to desorb over wide-spreading temperature region. Besides the desorption products common to BTBTT, imine ($EtN=CHMe$) can be formed via the β -H elimination of diethylamido. Accompanied by the formation of these species, hydrogen evolves continuously. Scheme 2 summarizes the decomposition of BTBDT. In both schemes, the continuous elimination of methyl groups at high temperature, an essential step leading to the formation of acetonitrile and hydrogen cyanide, remains the least understood part in the thermolysis of the precursors. Neither is it clear how solid tungsten nitrides are formed from the molecular skeletons whose formation forms the basis of the present work.

The stoichiometry of the formed tungsten nitride can be obtained from component-resolved XPS spectra in which the signals from the precursor can be differentiated from those of the coadsorbed amines. The elemental ratios of the final products are represented as $WN_{1.5}O_{0.1}C_{0.4}$ for BTBTT, and $WN_{1.3}O_{0.2}C_{0.8}$ for BTBDT. Carbon exists mostly in graphitic form with its C 1s b.e. at 284.6 eV, and a smaller amount of carbon may exist as carbonitride or carbide. The stoichiometry of our products is different from WN stoichiometry determined by Rutherford back-



Scheme 1. Proposed thermal decomposition pathways for BTBTT on Cu(111).



Scheme 2. Proposed thermal decomposition pathways for BTBDT on Cu(111).

scattering spectrometry in ALD growth from $(t\text{-BuN})_2\text{W}(\text{NMe}_2)_2$ [10]. The same study also showed that as-produced WN will convert to polycrystalline tungsten metal at an annealing condition of 1000 K for 30 min. Whether the oxygen is contained in tungsten oxynitride or tungsten oxide can be a matter of debate. However, we believe that oxynitride is perhaps a better description of the formed products based on the following arguments. The b.e. of W $4f_{7/2}$ for the trioxide (WO_3) is at a very high value of 35.8 eV, whereas the corresponding value for dioxide (WO_2) decreases to 32.8 eV [20]. The O 1s b.e. values for tungsten dioxide and trioxide are almost the same, 530.4 vs. 530.6 eV. If the oxide were to form, there seems to be no reason for the dioxide not to oxidize further into trioxide. However, we never observed any W $4f_{7/2}$ signal with b.e. higher than 35 eV; therefore, the formation of separate oxide does not seem to be the case.

5. Conclusion

We have investigated chemisorption and thermal decomposition of two tungsten nitride CVD precursors, BTBTT and BTBDT, on Cu(111) by means of TDS and SR-XPS. Molecularly intact chemisorption of two precursors on Cu(111) is possible at 100 K with W $4f_{7/2}$ at 34.0 eV. However, the thermal lability of the precursors manifests itself in a rapid decomposition at 300 K via the characteristic hydride abstraction/elimination pathways to produce stable surface intermediates identifiable by

curve-fitting XPS spectra. Two intermediates for each precursor are resolved. For BTBTT, one intermediate is $W(=NBu-t)_3$ and the other is a bridged amido complex, $[(t-BuN)_2W(\mu-NBu-t)]_2$. In comparison, a W-imine complex and a W–N–C metallacycle are two intermediates produced from BTBDT. Thermal desorption produces species that can be fully accounted for by considering the ligand chemistry alone. The desorption products from BTBTT include *t*-butylamine generated from α -H abstraction, isobutylene from γ -H elimination, acetonitrile from β -methyl elimination, and molecular hydrogen. In addition to these species, BTBDT produces one extra species of imine, $EtN=CHMe$, via β -H elimination. The eventual product after 800 K annealing is composed of tungsten nitrides incorporating oxygen and a small amount of graphitic carbons. Oxygen incorporation, driven by a large oxide formation enthalpy, depends on the level of moisture exposure. The formed nitride has a stoichiometry of $WN_{1.5}O_{0.1}C_{0.4}$ for BTBTT, and $WN_{1.3}O_{0.2}C_{0.8}$ for BTBDT.

Acknowledgement

YWY thank NSRRC for in-house equipment grant and National Science Council of ROC for Grant No. NSC89-2113-M-213-015.

References

- [1] T. Kodas, M. Hampden-Smith (Eds.), *The Chemistry of Metal CVD*, VCH, Weinheim, 1994.
- [2] G.B. Stringfellow, *Organometallic Vapor Phase Epitaxy: Theory and Practice*, Academic, New York, 1989.
- [3] M.L. Hitchman, K.F. Jensen (Eds.), *Chemical Vapor Deposition Principles and Applications*, London, Academic, 1993.
- [4] S.M. Gates, *Chem. Rev.* 96 (1996) 1519.
- [5] J.G. Ekerdt, Y.-M. Sun, A. Szabo, G.J. Szulczewski, J.M. White, *Chem. Rev.* 96 (1996) 1499.
- [6] J.P. Endle, Y.-M. Sun, J.M. White, J.G. Ekerdt, *J. Vac. Sci. Technol. A* 16 (1998) 1262.
- [7] S. Bocharov, Z. Zhang, T.P. Beebe Jr., A.V. Teplyakov, *Thin Solid Films* 471 (2005) 159.
- [8] B.L. Park et al., *J. Electron Mater.* 26 (1997) L1.
- [9] R.R. Ivanova, C.J. Galewski, C.A. Sans, T.E. Seidel, S. Grunow, K. Kumar, A.E. Kaloyeros, *Mater. Res. Soc. Symp. Proc.* 564 (1999) 321.
- [10] J.S. Becker, S. Suh, S. Wang, R.G. Gordon, *Chem. Mater.* 15 (2003) 2969.
- [11] H.T. Chiu, S.H. Chuang, *J. Mater. Res.* 8 (1993) 1353.
- [12] E.L. Crane, H.-T. Chiu, R.G. Nuzzo, *J. Phys. Chem. B* 105 (2001) 3549.
- [13] J.-B. Wu, Y.-W. Yang, Y.-F. Lin, H.-T. Chiu, *J. Vac. Sci. Technol. A* 21 (2003) 1620.
- [14] J.-B. Wu, Y.-W. Yang, Y.-F. Lin, H.-T. Chiu, *J. Phys. Chem. B* 108 (2004) 1677.
- [15] E.R. Malinowski, *Factor Analysis in Chemistry*, Wiley & Sons, New York, 1991.
- [16] H.-T. Chiu, S.-H. Chuang, C.-E. Tsai, G.-H. Lee, S.-M. Peng, *Polyhedron* 17 (1998) 2187.
- [17] G. Anger, A. Winker, K.D. Rendulic, *Surf. Sci.* 220 (1989) 1.
- [18] P.B. Lloyd, M. Swaminathan, J.W. Kress, B.J. Tatarchuk, *Appl. Surf. Sci.* 119 (1997) 267.
- [19] K. Inamura, Y. Inoue, S. Ikeda, K. Kishi, *Surf. Sci.* 155 (1985) 173.
- [20] J.F. Moulder, W.F. Stickle, P.E. Sobol, K.D. Bomben, *Handbook of X-ray Photoelectron Spectroscopy*, Perkin-Elmer Corp., Eden Prairie, MN, 1992.
- [21] A.K. Sharma, P. Ayyub, M.S. Multani, K.P. Adhi, S.B. Ogale, M. Sunderaraman, D.D. Upadhyay, S. Banerjee, *Appl. Phys. Lett.* 69 (1996) 3489.
- [22] J.M. Ripalda, I. Montero, L. Galan, *Diamond Relat. Mater.* 7 (1998) 402.
- [23] Å. Johansson, S. Stafström, *J. Chem. Phys.* 111 (1999) 3203.
- [24] L. Galan, I. Monte, F. Rueda, *Surf. Coat. Technol.* 83 (1996) 103.
- [25] NIST Chemistry WebBook.
- [26] D.M. Riffe, G.K. Wertheim, P.H. Citrin, *Phys. Rev. Lett.* 63 (1989) 1976.
- [27] T.-W. Pi, I.-H. Hong, C.-P. Cheng, *Phys. Rev. B* 58 (1998) 4149.
- [28] J. Cheon, D.M. Rogers, G.S. Girolami, *J. Am. Chem. Soc.* 119 (1997) 6804.
- [29] F. Zaera, S. Tjandra, *J. Am. Chem. Soc.* 118 (1996) 12738.
- [30] K.W. Chiu, R.A. Jones, G. Wilkinson, A.M.R. Galas, M.B. Hursthouse, *J. Chem. Soc., Dalton Trans.* 10 (1981) 2088.
- [31] A. Mayr, C.M. Bastos, *J. Am. Chem. Soc.* 112 (1990) 7797.
- [32] R.M. Fix, R.G. Gordon, D.M. Hoffman, *Chem. Mater.* 2 (1990) 235.
- [33] C.M. Truong, P.J. Chen, J.S. Corneille, W.S. Oh, D.W. Goodman, *J. Phys. Chem.* 99 (1995) 8831.
- [34] G. Ruhl, R. Rehm, M. Knížová, R. Merica, S. Veprek, *Chem. Mater.* 8 (1996) 2712.
- [35] J. Cheon, L.H. Dubois, G.S. Girolami, *J. Am. Chem. Soc.* 119 (1997) 6814.
- [36] Y.-D. Wu, Z.-H. Peng, Z. Xue, *J. Am. Chem. Soc.* 118 (1996) 9772.
- [37] T.R. Cundari, J.M. Morse Jr., *Chem. Mater.* 8 (1996) 189.
- [38] L.H. Dubois, B.R. Zegarski, G.S. Girolami, *J. Electrochem. Soc.* 139 (1992) 3603.
- [39] F. Ossola, F. Maury, *Chem. Vapor Depos.* 3 (1997) 137.
- [40] J.-B. Wu, Y.-F. Lin, J.-L. Wang, P.-J. Chang, C.-P. Tasi, C.-C. Lu, H.-T. Chiu, Y.-W. Yang, *Inorg. Chem.* 42 (2003) 4516.
- [41] T.J. Chuang, Y.L. Chan, P. Chuang, R. Klauser, *J. Electron Spectrosc. Relat. Phenom.* 98/99 (1999) 149.
- [42] G. Soto, W. de la Cruz, F.F. Castillón, J.A. Díaz, R. Machorro, M.H. Fariás, *Appl. Surf. Sci.* 214 (2003) 58.